JACS
JOURNAL OF THE AMERICAN CHEMICAL SOCIETY

Communication

pubs.acs.org/JACS

Yolk–Shell Nanocrystal@ZIF-8 Nanostructures for Gas-Phase Heterogeneous Catalysis with Selectivity Control

Chun-Hong Kuo, Yang Tang, Lien-Yang Chou, Brian T. Sneed, Casey N. Brodsky, Zipeng Zhao, and Chia-Kuang Tsung*

Department of Chemistry, Merkert Chemistry Center, Boston College, 2609 Beacon Street, Chestnut Hill, Massachusetts 02467, United States

Supporting Information

ABSTRACT: A general synthetic strategy for yolk–shell nanocrystal@ZIF-8 nanostructures has been developed. The yolk–shell nanostructures possess the functions of nanoparticle cores, microporous shells, and a cavity in between, which offer great potential in heterogeneous catalysis. The synthetic strategy involved first coating the nanocrystal cores with a layer of Cu_2O as the sacrificial template and then a layer of polycrystalline ZIF-8. The clean Cu_2O surface assists in the formation of the ZIF-8 coating layer and is etched off spontaneously and simultaneously during this process. The yolk–shell nanostructures were characterized by transmission electron microscopy, scanning electron microscopy, X-ray diffraction, and nitrogen adsorption. To study the catalytic behavior, hydrogenations of ethylene, cyclohexene, and cyclooctene as model reactions were carried out over the Pd@ZIF-8 catalysts. The microporous ZIF-8 shell provides excellent molecular-size selectivity. The results show high activity for the ethylene and cyclohexene hydrogenations but not in the cyclooctene hydrogenation. Different activation energies for cyclohexene hydrogenation were obtained for nanostructures with and without the cavity in between the core and the shell. This demonstrates the importance of controlling the cavity because of its influence on the catalysis.

Yolk–shell nanostructures have generated recent research interest because of their potential applications in heterogeneous catalysis,[1] photocatalysis,[2] and biomedicine.[3,4] Integrating the functions of the nanocrystal core, the nanostructured shell, and the cavity in between provides a tool for optimizing the performance of a nanomaterial. In a yolk–shell catalyst, the metal core provides a catalytically active surface for the reaction and the porous shell serves as a barrier layer to prevent aggregation of the active surface with neighboring metal cores during the reaction. Compared with the core–shell nanostructure,[5] in which the shell is directly on the metal surface, the cavity between the core and the shell in the yolk–shell structure not only reserves a larger exposed metal surface for the reactants but also makes the reactants interact with the surface more homogeneously. It has been proposed that the shell in the yolk–shell structure could introduce multiple functions into the catalyst, such as regulation of diffusion and control of molecular-size selectivity; however, in most of the previous yolk–shell catalysts, the shell has served only one function, acting as a protective layer to prevent aggregation between particles during the reaction.[6−13] This is mainly because in previous works, the shell materials were limited to nonordered porous materials, restricting the functions of the shells. Here we report a general method for the synthesis of yolk–shell structures with metal–organic framework (MOF) shells. The uniform and controllable microporous structure, large internal surface area, and tunable chemical properties of the MOF shell could introduce new functions into the yolk–shell nanostructures, making them more attractive for different applications. We chose zeolitic imidazolate framework 8 (ZIF-8) as the shell material to demonstrate our method. ZIF-8, a subclass of MOFs, has high thermal and chemical stability.[14] It is one of the few commercially available MOFs because of its great potential in gas separation[15−17] and gas storage.[18,19]

Most of the previously reported synthetic strategies for incorporating nanocrystals into MOFs, such as those used for Au@ZIF-8[20,21] and Cu/ZnO@MOF-5,[22] have used gas-phase infiltration or grinding. These postsynthesis incorporation methods cannot create the cavity around the nanocrystal core, and the morphology of the nanocrystal core is uncontrollable. The morphology is a very important factor in the function of nanocrystals for catalytic and optical properties. Furthermore, in these methods, the porous structure of the MOF was sometimes damaged during the incorporation, and some of the nanocrystals were found on the external surface of the MOF. A preferred strategy, coating the MOF on the preformed nanocrystals, was recently reported, but the synthesis of MOF yolk–shell nanostructures is still challenging.[23] In this work, we developed a new synthetic strategy in which metal nanocrystals are first coated with a layer of a sacrificial template and then coated with ZIF-8 (Scheme 1). We specifically choose Cu_2O as the sacrificial template. Not only can the Cu_2O be etched simultaneously and spontaneously by the protons generated during the formation of ZIF-8, but also, the capping-agent-free surface of Cu_2O provides a clean surface for ZIF-8 coating. Also, methods of Cu_2O coating on different nanocrystals have been well-developed, which makes our synthetic strategy general and versatile.[24]

Typical single shape-controlled metal nanocrystals incorporated in crack-free polycrystalline ZIF-8 crystals are shown in

Received: July 13, 2012
Published: August 17, 2012

   dx.doi.org/10.1021/ja306869j | J. Am. Chem. Soc. 2012, 134, 14345−14348

Scheme 1. Growth Procedure for the Nanocrystal@ZIF-8 Yolk–Shell Nanostructures

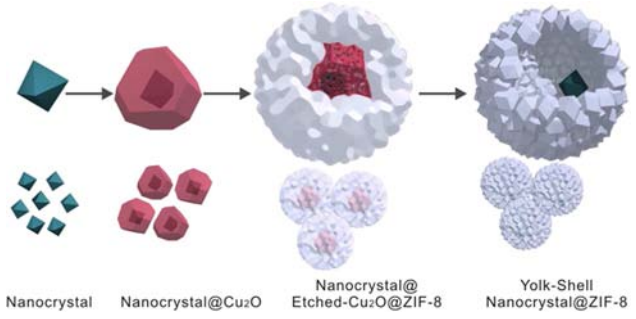

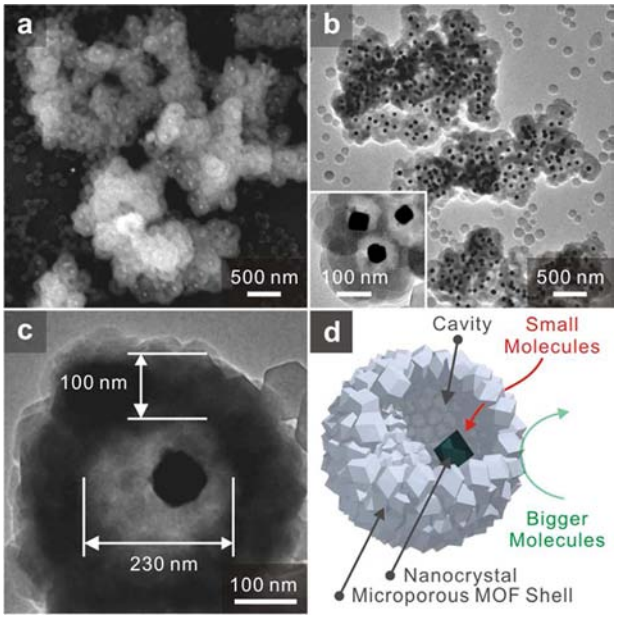

Figure 1. Nanocrystal@ZIF-8 yolk–shell nanostructures. (a) SEM and (b, c) TEM images. The cores are Pd octahedra with edge sizes of 60 nm, and the shells are microporous ZIF-8 with thickness of ~100 nm. (d) Schematic sketch of the yolk–shell nanostructure.

Figure 1 and Figure S1 in the Supporting Information (SI). The shapes and sizes of the nanocrystals were well-maintained during the synthesis. All of the nanocrystals were incorporated in ZIF-8. A small number of ZIF-8 crystals containing no metal nanocrystals were also formed and could be removed by centrifugation. To demonstrate that we can preserve the size and shape of the nanocrystals by using this strategy, relatively large shape-controlled metal nanocrystals were used. The same method could be applied to different sized nanocrystals. In a typical synthesis, Pd octahedra[25] were coated with Cu_2O to form a Pd@Cu_2O core–shell structure (Figure S2a). After Cu_2O coating, the Pd@Cu_2O structures were mixed with the ZIF-8 precursors 2-methylimidazole (2-meIm) and zinc nitrate in methanol.[26] As the pH of the solution decreased from 7 to 5 because of the deprotonation of 2-meIm during the formation of ZIF-8, the Cu_2O was etched off simultaneously.[10] A trace amount of the Cu_2O residue was observed (Figure S2b). A solution of 3% NH_4OH in methanol was used to remove the trace amount of residual Cu_2O in the final step. The products were then washed with methanol and collected by centrifugation. The absence of the Cu signal in the elemental analysis (ICP-AES) confirmed the removal of Cu_2O from the final products. The scanning electron microscopy (SEM) and transmission electron microscopy (TEM) images in Figure 1 show that the Pd nanocrystals were well-separated by the ZIF-8 shells. The Figure 1b inset clearly shows the well-preserved morphology of the nanocrystals after the coating as well as the cavity. The thickness of the ZIF-8 shell was ~100 nm, and the ZIF-8 was polycrystalline and crack-free, as further confirmed by the catalysis results discussed below. The solution colors of these samples at different stages are shown in Figure S3. After the Pd nanocrystals were coated with Cu_2O, the color changed from brown to green, indicating the formation of Cu_2O shells.[24] During the ZIF-8 coating, the color gradually turned back to brown, but the mixture was turbid, indicating the depletion of Cu_2O and the simultaneous formation of ZIF-8.

The crystal structure and porosity of the shell were studied by powder X-ray diffraction (PXRD) and nitrogen-sorption measurements. The PXRD patterns of pure ZIF-8 and the Pd@ZIF-8 yolk–shell nanostructure are shown in Figure 2a. Patterns generated by the ordered porous structure of the ZIF-8 shells (2θ = 5–35°)[27] and the Pd cores (2θ = 35–85°) were both observed for the Pd@ZIF-8 yolk–shell nanostructure. All of the prominent peaks for the ZIF-8 shells, including

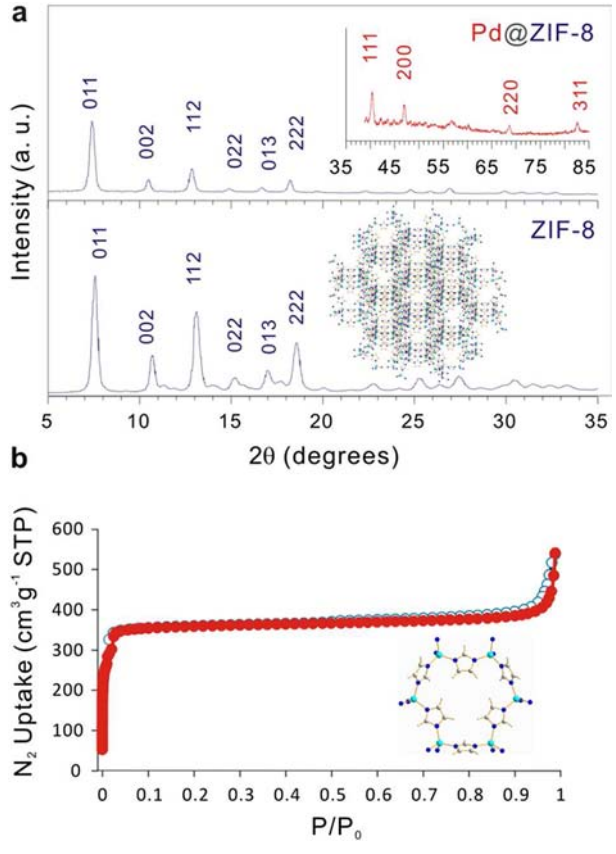

Figure 2. Crystal and pore structures of the Pd@ZIF-8 yolk–shell nanostructure. (a) PXRD patterns of the yolk–shell nanostructure and pure ZIF-8 crystals. The peaks of the ZIF-8 shells (upper) correspond to those of pure ZIF-8 nanocrystals, revealing that the ZIF-8 shells had the same crystal structure as the pure ZIF-8 crystals. The inset shows the higher-angle diffraction peaks contributed by the Pd octahedra. (b) Nitrogen adsorption–desorption isotherm of the Pd@ZIF-8 yolk–shell nanostructure, showing type-I behavior and confirming the microporous structure of the ZIF-8 shells. The BET surface area was 1396 m^2/g.

dx.doi.org/10.1021/ja306869j | J. Am. Chem. Soc. 2012, 134, 14345–14348

011, 002, 112, 022, 013, and 222, corresponded to those of pure ZIF-8 crystals. This confirmed the sodalite zeolite-type crystal structure of the ZIF-8 shell, and the well-defined peaks revealed the high crystallinity. The nitrogen adsorption–desorption isotherm of the Pd@ZIF-8 yolk–shell nanostructure (Figure 2b) displayed type-I behavior. The steep step at low relative pressure revealed that the shells were microporous. The specific surface area estimated by the Brunauer–Emmett–Teller (BET) method was 1396 m^2/g. The lower surface area of the yolk–shell structure compared with pure ZIF-8 (1643 m^2/g)[23] is mainly due to the heavier and nonporous metal cores. The thermal stability of the yolk–shell structure was characterized by thermogravimetric analysis (TGA) (Figure S4). The decomposition temperature of Pd@ZIF-8 yolk–shell nanostructure was 425 °C, which is only marginally lower than that of pure ZIF-8 crystals (470 °C). This difference can be attributed to the difference in the crystal sizes of the ZIF-8 shells and the few hundred nanometer pure ZIF-8 crystals.

Gas-phase hydrogenations of ethylene, cyclohexene, and cyclooctene were carried out to study the molecular-size selectivity of the catalysis (Scheme 2). Catalysts consisting of

Scheme 2. Molecular-Size-Selective Catalysis

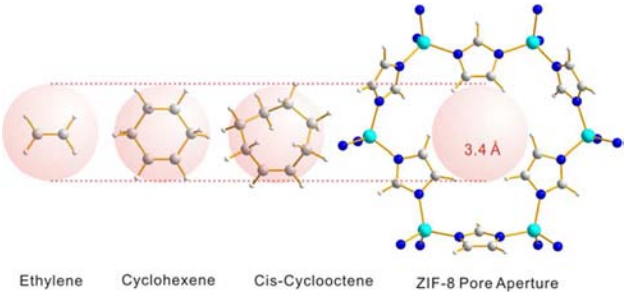

60 nm Pd nanocrystal@ZIF-8 yolk–shell nanostructures (yolk–shell Pd@ZIF-8), 60 nm Pd nanocrystals directly deposited on ZIF-8 crystal surfaces (Pd on ZIF-8), and 20 nm Pd nanocrystals coated with ZIF-8 layers without a cavity (core–shell Pd@ZIF-8) were prepared for comparison. Table 1 shows the activities and activation energies of the reactions. For

Table 1. Catalytic Behavior of Different ZIF-8 Nanostructures[a]

	core–shell Pd@ZIF-8	yolk–shell Pd@ZIF-8	Pd on ZIF-8
Ethylene Hydrogenation[a]			
activity ($mol \cdot g_{Pd}^{-1} \cdot s^{-1}$)[b]	1.3×10^{-2}	3.2×10^{-3}	3.0×10^{-3}
E_a (kJ/mol)[c]	41.7	42.7	41.0
Cyclohexene Hydrogenation[a]			
activity ($mol \cdot g_{Pd}^{-1} \cdot s^{-1}$)[b]	1.5×10^{-4}	3.2×10^{-5}	2.8×10^{-5}
TOF (s^{-1})[d]	0.27	0.23	0.21
E_a (kJ/mol)[c]	27.5	40.1	41.1
Cyclooctene Hydrogenation[a]			
activity ($mol \cdot g_{Pd}^{-1} \cdot s^{-1}$)[b]	N/A	N/A	2.8×10^{-6}
TOF (s^{-1})[d]	N/A	N/A	0.02
E_a (kJ/mol)[c]	N/A	N/A	34.9

[a]Conditions in each experiment: 10 Torr hydrocarbon (C_2H_4, C_6H_4, or C_8H_{14}), 100 Torr H_2, and 650 Torr He at 323 K. [b]The metal loading was determined by elemental analysis and used to normalize the conversion by the mass of Pd. [c]Arrhenius activation energy. [d]Turnover frequency.

ethylene hydrogenation, all of the catalysts showed high activity and similar activation energies, indicating that the same ethylene hydrogenation kinetics occurred and also that there was no significant diffusional influence caused by the ZIF-8 shells. The activity difference was mainly due to the size difference of the Pd nanocrystals. Using the same nanocrystals in different catalysts is challenging because the core–shell synthetic strategy is different from the yolk–shell strategy; however, after the results were normalized by the Pd surface area, the activities were similar. For the cyclooctene hydrogenation, both the core–shell and yolk–shell catalysts showed no detectable activity, but the Pd on ZIF-8 catalyst showed good activity. This result clearly demonstrates the molecule-size-selective property of the ZIF-8 shell. Ethylene molecules (2.5 Å) are small enough to diffuse through the pore apertures of the ZIF-8 shells (3.4 Å) without serious hindrance; however, the cyclooctene molecules (5.5 Å) are much bigger than the pore apertures. Therefore, only the catalyst in which the Pd nanocrystals were directly deposited on the external surface of ZIF-8 (Pd on ZIF-8) showed activity for cyclooctene hydrogenation. This result also clearly suggests that the ZIF-8 shells in both the yolk–shell and core–shell structures were devoid of cracks or fractures. No significant deactivation was observed even when the catalysts were heated to 150 °C. The catalysts were checked by TEM after the reactions, and most of them still maintained the yolk–shell structure.

Cyclohexene hydrogenation displayed very interesting catalytic phenomena in this series of hydrogenation reactions. Although the size of cyclohexene molecules (4.2 Å) is comparable to the aperture size of ZIF-8, all of the catalysts showed good activities for cyclohexene hydrogenation. This indicates the flexibility of the ZIF-8 framework.[28] The yolk–shell Pd@ZIF-8 catalyst and Pd on ZIF-8 had similar activation energies. The core–shell Pd@ZIF-8 catalyst had a lower activation energy. To exclude the chance that the activation energy difference resulted from capping agents or supports, a series of Pd nanocrystals were prepared using different capping agents and then directly deposited on different supports. Table S1 in the SI shows the activation energies for all of the catalysts. The values of the activation energies were all ~40 kJ/mol except that for the core–shell Pd@ZIF-8 catalyst, which was lower (27 kJ/mol). The observation of a lower activation energy could be generated for different reasons. It is known that the internal diffusion influence can lead to a change in measured activation energy.[29,30] Although it is not conclusive enough to use values of activation energy alone to explain diffusional influence, the comparable sizes of the pore aperture and cyclohexene make the transport limitation highly possible. The diffusion through the core–shell catalyst is mainly configurational diffusion, whereas the diffusion through the yolk–shell catalyst is a combination of configurational diffusion (shell) and Knudsen diffusion (cavity). This could result in different catalytic behaviors. The other possibility is the kinetics difference due to the conformation of the molecules on the metal surface. The size of a cyclohexene molecule in its most stable conformation, ~4.2 Å, is comparable to the size of the aperture (3.4 Å). Thus, the cyclohexene molecules could interact with the Pd surface only by successive variations in their conformations in the case of the core–shell structure, in which the ZIF-8 is directly on the Pd surface. It has been shown that the hydrogenation kinetics for six-membered carbon rings can be affected by the conformation of the molecules on the metal surface.[31] Detailed studies of the reactions for further

dx.doi.org/10.1021/ja306869j | J. Am. Chem. Soc. 2012, 134, 14345–14348

understanding the activation energy change are currently underway, but the study here clearly indicates the importance of the ability to control the cavity for reactions. The ability to create the yolk–shell catalysts provides a strategy to perform selective catalysis without changing the kinetics or generating a diffusional influence.

In conclusion, we have developed a general strategy for the synthesis of nanocrystal@ZIF-8 yolk–shell nanostructures. Cu_2O is used as a sacrificial template because it can be etched simultaneously and spontaneously during the formation of ZIF-8. The nanostructures were applied as catalysts for the gas-phase hydrogenations of ethylene, cyclohexene, and cyclooctene. The ZIF-8 shell showed interesting size selectivity in ethylene hydrogenation versus cyclooctene hydrogenation. For cyclohexene hydrogenation, the measured activation energy for the yolk–shell nanostructure was different from that for the core–shell nanostructure, which demonstrates the influence of the cavity structure in the yolk–shell structure. Integrating the functions of the nanocrystal core, the microporous shell, and the cavity in between provides a new tool for creating selective heterogeneous catalysts.

■ ASSOCIATED CONTENT

Supporting Information

Detailed experimental procedures; TEM images of Pd cube@ZIF-8, Pt small particle@ZIF-8, and Au octahedron@ZIF-8 yolk–shell structures; XRD patterns, photographs, and TEM images of the samples at different synthetic stages; TGA data; and a table of activation energies for cyclohexene hydrogenation. This material is available free of charge via the Internet at http://pubs.acs.org.

■ AUTHOR INFORMATION

Corresponding Author

frank.tsung@bc.edu

Notes

The authors declare no competing financial interest.

■ ACKNOWLEDGMENTS

The research was funded by Boston College. C.-H.K. thanks the National Science Council of Taiwan for offering the scholarship.

■ REFERENCES

(1) Ikeda, S.; Ishino, S.; Harada, T.; Okamoto, N.; Sakata, T.; Mori, H.; Kuwabata, S.; Torimoto, T.; Matsumura, M. *Angew. Chem., Int. Ed.* **2006**, *45*, 7063.
(2) Lee, I.; Joo, J. B.; Yin, Y. D.; Zaera, F. *Angew. Chem., Int. Ed.* **2011**, *50*, 10208.
(3) Zhang, L.; Qiao, S. Z.; Jin, Y. G.; Chen, Z. G.; Gu, H. C.; Lu, G. Q. *Adv. Mater.* **2008**, *20*, 805.
(4) Gao, J. H.; Liang, G. L.; Cheung, J. S.; Pan, Y.; Kuang, Y.; Zhao, F.; Zhang, B.; Zhang, X. X.; Wu, E. X.; Xu, B. *J. Am. Chem. Soc.* **2008**, *130*, 11828.
(5) Joo, S. H.; Park, J. Y.; Tsung, C.-K.; Yamada, Y.; Yang, P.; Somorjai, G. A. *Nat. Mater.* **2009**, *8*, 126.
(6) Yang, Y.; Liu, J.; Li, X.; Liu, X.; Yang, Q. *Chem. Mater.* **2011**, *23*, 3676.
(7) Lee, J.; Park, J. C.; Song, H. *Adv. Mater.* **2008**, *20*, 1523.
(8) Liu, J.; Qiao, S. Z.; Hartono, S. B.; Lu, G. Q. *Angew. Chem., Int. Ed.* **2010**, *49*, 4981.
(9) Yin, Y. D.; Rioux, R. M.; Erdonmez, C. K.; Hughes, S.; Somorjai, G. A.; Alivisatos, A. P. *Science* **2004**, *304*, 711.
(10) Kuo, C. H.; Huang, M. H. *J. Am. Chem. Soc.* **2008**, *130*, 12815.
(11) Wu, X. J.; Xu, D. S. *J. Am. Chem. Soc.* **2009**, *131*, 2774.
(12) Wu, X. J.; Xu, D. S. *Adv. Mater.* **2010**, *22*, 1516.
(13) Güttel, R.; Paul, M.; Schüth, F. *Catal. Sci. Technol.* **2011**, *1*, 65.
(14) Phan, A.; Doonan, C. J.; Uribe-Romo, F. J.; Knobler, C. B.; O'Keeffe, M.; Yaghi, O. M. *Acc. Chem. Res.* **2010**, *43*, 58.
(15) Li, K. H.; Olson, D. H.; Seidel, J.; Emge, T. J.; Gong, H. W.; Zeng, H. P.; Li, J. *J. Am. Chem. Soc.* **2009**, *131*, 10368.
(16) Venna, S. R.; Carreon, M. A. *J. Am. Chem. Soc.* **2010**, *132*, 76.
(17) Bux, H.; Feldhoff, A.; Cravillon, J.; Wiebcke, M.; Li, Y. S.; Caro, J. *Chem. Mater.* **2011**, *23*, 2262.
(18) Wu, H.; Zhou, W.; Yildirim, T. *J. Am. Chem. Soc.* **2007**, *129*, 5314.
(19) Banerjee, R.; Phan, A.; Wang, B.; Knobler, C.; Furukawa, H.; O'Keeffe, M.; Yaghi, O. M. *Science* **2008**, *319*, 939.
(20) Jiang, H. L.; Liu, B.; Akita, T.; Haruta, M.; Sakurai, H.; Xu, Q. *J. Am. Chem. Soc.* **2009**, *131*, 11302.
(21) Esken, D.; Turner, S.; Lebedev, O. I.; Van Tendeloo, G.; Fischer, R. A. *Chem. Mater.* **2010**, *22*, 6393.
(22) Muller, M.; Hermes, S.; Kaehler, K.; van den Berg, M. W. E.; Muhler, M.; Fischer, R. A. *Chem. Mater.* **2008**, *20*, 4576.
(23) Lu, G.; Li, S.; Guo, Z.; Farha, O. K.; Hauser, B. G.; Qi, X.; Wang, Y.; Wang, X.; Han, S.; Liu, X.; DuChene, J. S.; Zhang, H.; Zhang, Q.; Chen, X.; Ma, J.; Loo, S. C. J.; Wei, D. W.; Yang, Y.; Hupp, J. T.; Huo, F. *Nat. Chem.* **2012**, *4*, 310.
(24) Kuo, C. H.; Hua, T. E.; Huang, M. H. *J. Am. Chem. Soc.* **2009**, *131*, 17871.
(25) Niu, W. X.; Zhang, L.; Xu, G. B. *ACS Nano* **2010**, *4*, 1987.
(26) Moh, P. Y.; Cubillas, P.; Anderson, M. W.; Attfield, M. P. *J. Am. Chem. Soc.* **2011**, *133*, 13304.
(27) Venna, S. R.; Jasinski, J. B.; Carreon, M. A. *J. Am. Chem. Soc.* **2010**, *132*, 18030.
(28) Fairen-Jimenez, D.; Moggach, S. A.; Wharmby, M. T.; Wright, P. A.; Parsons, S.; Düren, T. *J. Am. Chem. Soc.* **2011**, *133*, 8900.
(29) Mears, D. E. *Ind. Eng. Chem. Process Des. Dev.* **1971**, *10*, 541.
(30) Madon, R. J.; Boudart, M. *Ind. Eng. Chem. Fundam.* **1982**, *21*, 438.
(31) Bratlie, K. M.; Kliewer, C. J.; Somorjai, G. A. *J. Phys. Chem. B* **2006**, *110*, 17925.